The Spatiotemporal Transmission Dynamics of COVID-19 among Multiple Regions: A Modeling Study in China

Qiaojuan Jia
Guilin University of Electronic Technology
Jiali Li
Guilin University of Electronic Technology
Hualiang Lin
Sun Yat-Sen University
Fei Tian
Sun Yat-Sen University
Guanghu Zhu (ghzhu@guet.edu.cn)
Guilin University of Electronic Technology https://orcid.org/0000-0002-1416-1476

Research Article

Keywords: COVID-19, spatiotemporal transmission, human mobility, prevention and control, reproduction number

Posted Date: July 29th, 2021

DOI: https://doi.org/10.21203/rs.3.rs-742722/v1

Version of Record: A version of this preprint was published at Nonlinear Dynamics on October 29th, 2021. See the published version at https://doi.org/10.1007/s11071-021-07001-1.

The spatiotemporal transmission dynamics of COVID-19 among multiple regions: A modeling study in China

Qiaojuan Jia[1], Jiali Li[1], Hualiang Lin[2], Fei Tian[2], Guanghu Zhu[1,*],
1 School of Mathematics and Computing Science, Guilin University of Electronic Technology, Guilin, China
2 Department of Epidemiology, School of Public Health, Sun Yat-sen University, Guangzhou, 510080, China
***ghzhu@guet.edu.cn**

Abstract

Current explosive outbreak of COVID-19 around the world is a complex spatiotemporal process with hidden interactions between viruses and humans. This study aims at clarifying the transmission patterns and the driving mechanism that contributed to the COVID-19 epidemics across the provinces of China. Thus a new dynamical transmission model is established by ordinary differential system. The model takes into account the hidden circulation of COVID-19 virus among/within humans, which incorporates the spatial diffusion of infection by parameterizing human mobility. Theoretical analysis indicates that the basic reproduction number is a unique epidemic threshold, which can unite infectivity in each region by human mobility, and can totally determine whether COVID-19 proceeds among multiple regions. By validating the model with real epidemic data in China, it is found that (1) if without any intervention, COVID-19 would overrun China within three months, resulting in more than 1.1 billion infections; (2) high frequency of human mobility can trigger COVID-19 diffusion across each province in China, no matter where the initial infection locates; (3) travel restrictions and other non-pharmaceutical interventions must be implemented simultaneously for disease control; and (4) infection sites in central and east (rather than west and northeast) of China would easily stimulate quick diffusion of COVID-19 in the whole country.

Key words COVID-19, spatiotemporal transmission, human mobility, prevention and control, reproduction number

1 Introduction

The pandemic coronavirus disease (COVID-19) is caused by a newly discovered coronavirus called SARS-CoV-2, which can spread from an infected person's mouth or nose in small liquid particles when they cough, sneeze, speak, sing or breathe [1]. Such easy transmission routes coupled with large human mobility quickly result in explosive outbreak across the world. As of June 10, 2021, this disease has attacked 212 countries, with a total of over 170 million confirmed cases and over 3.76 million deaths [1]. COVID-19 is disrupting global health, economic, political and social systems, and is posing comprehensive threats to people around the world.

The ongoing COVID-19 pandemic exhibits a clear time-space evolution. As the first case was reported in Wuhan, China on 29 December 2019, the disease has spread to all the provinces in China within a month [2]. By 21 February 2020, it has occurred in 27 countries, and the number of infected countries quickly increases to over 170 in late March. The infection size rose sharply from 282 to over 5 million during 5 months period. Such fast diffusion and hierarchical structures in time and place were possibly shaped by human behaviors (e.g., communication, work and movement). For example, after initial emergence in China, travel-related cases started appearing in other parts of the world with strong travel links to Wuhan [3]. This pattern along with the special

characteristics of COVID-19: (1) high pathogenicity and hidden transmission among humans [4], (2) large asymptomatic patients with infectivity [5], (3) short serial interval [6], and (4) massive susceptibility [7], make it very difficult to assess the risk and control the infection. Recognizing the spatiotemporal transmission dynamics can help to forecast epidemic tendency, identify the potential drivers of transmission and high-risk population, and guide the designing of targeted interventions in resource limited settings.

Technically speaking, pure statistical model and mapping analysis can quantitatively tell the infection patterns in time and space. Mathematical frameworks incorporated epidemiology survey data can further capture the intrinsic variability of spatiotemporal transmission of epidemics, which are used increasingly in interdisciplinary studies [8]. Focusing on in the COVID-19 pandemic, many epidemiology-inspired models, including SIR, SIS, and SEIR models, had been built to study the spreading patterns [9, 10, 11, 12, 13, 14]. By simulating the underlying transmission process, these studies found that (1) real-time mobility data from Wuhan can well elucidate the transmission in cities across China (2) various nonpharmaceutical interventions are effective in controlling the spread of the disease [13, 15, 16, 17, 18]; and (3) mobility networks of air travel can predict the global diffusion pattern at the early stages of the outbreak, and an unconstrained mobility would have significantly accelerated the spreading of COVID-19 [19].

This paper goes a further step to provide a new modeling framework with consideration of human mobility and surveillance data to clarify the hidden dynamics accounting for COVID-19 spatiotemporal transmission in China. Based on the deterministic compartment model, a multi-population transmission model of COVID-19 is established by ordinary differential equations (ODE). Qualitative theory is used to analyze the propagation dynamics of the model, including the expression of the basic reproduction number and the equilibria, the global stability of the disease-free and endemic equilibria. Finally, this model is applied to investigate the detailed transmission patterns of COVID-19 across the provinces in China.

2 Modeling framework

To simulate the spatiotemporal transmission of COVID-19 across different regions, a new meta-population dynamic model is proposed in this section. Based on the epidemiology features of COVID-19 and compartmental theory, the following basic assumptions are proposed.

- During the outbreak of COVID-19 infection, humans are divided into susceptible (S_i), exposed (E_i), preclinical infectious (I_i^p), subclinical infectious (I_i^s), clinical infectious (I_i^c) and recovered (R_i) classes. Here I_i^p and I_i^s are inapparent infections, and I_i^c are apparent infections. The sum of these classes constitute the total population size, that is, $N_i = S_i + E_i + I_i^p + I_i^s + I_i^c + R_i$. It is assumed that N_i is a constant, in which birth rate equals to death rate d. Here the subscript i denote the location of these parameters.

- The infection routes follows susceptible-latent-infected-recovered process. Individuals can be infected through contact with infectious individuals and then experience an incubation period $1/\eta$. Exposed individuals progress to preclinical infectious (with probability ϕ) and subclinical infectious (with probability $1-\phi$), subclinical infections with mild or no symptoms could not be easily found and treated, but they can self-recover after time $1/\gamma$. Preclinical infections before symptom appear progress to become clinical infectious who develop symptoms after time $1/\delta$. They receive treatment and are cured successful through time $1/\omega$.

- When novel coronavirus carried by infected humans invades into a virgin area people there (local residents and visitors from other region) could be infected with certain probability. The model takes into account such spatial diffusion by incorporating a migration matrix P, in which element P_{ij} denotes the average duration per unit time that the residents in region i stay in region j. It satisfies $P_{ij} \geq 0$ and $\sum_j P_{ij} = 1$.

Based on the above assumption, the essential features of the model framwork are depicted in Figure 1. Accordingly, the governing equations for simulating the spatiotemporal transmission dynamics

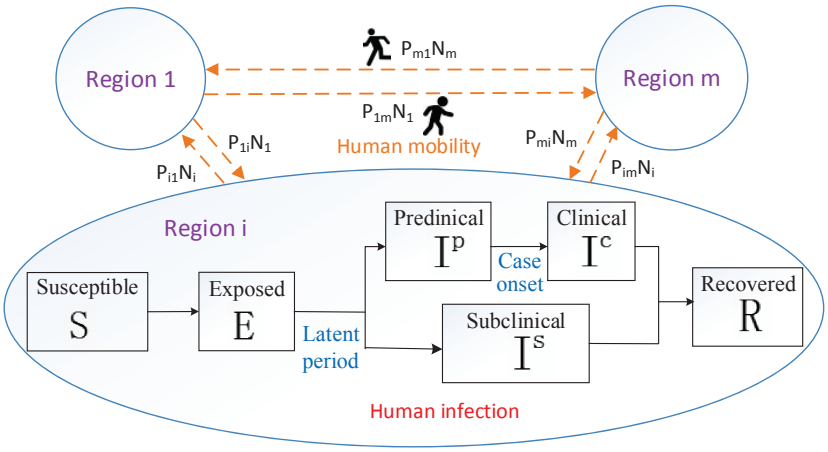

Figure 1: Flow diagram on COVID-19 transmission with humans mobility among different regions.

of COVID-19 are illustrated as follows:

$$
\begin{cases}
\dfrac{dS_i}{dt} = dN_i - \displaystyle\sum_{j=1}^{n} \lambda_j P_{ij} S_i \frac{\sum_{k=1}^{n} P_{kj}\left(I_k^p + \alpha I_k^s + \beta I_k^c\right)}{\sum_{k=1}^{n} P_{kj} N_k} - dS_i, \\
\dfrac{dE_i}{dt} = \displaystyle\sum_{j=1}^{n} \lambda_j P_{ij} S_i \frac{\sum_{k=1}^{n} P_{kj}\left(I_k^p + \alpha I_k^s + \beta I_k^c\right)}{\sum_{k=1}^{n} P_{kj} N_k} - (\eta + d)E_i, \\
\dfrac{dI_i^p}{dt} = \phi\eta E_i - (\delta + d)I_i^p, \\
\dfrac{dI_i^s}{dt} = (1-\phi)\eta E_i - (\gamma + d)I_i^s, \\
\dfrac{dI_i^c}{dt} = \delta I_i^p - (\omega + d)I_i^c, \\
\dfrac{dR_i}{dt} = \gamma I_i^s + \omega I_i^c - dR_i,
\end{cases}
\tag{1}
$$

where λ_j is the specific transmission rate in region j. The interpretation of other model parameters are presented in Table 1.

Table 1: **Description of parameters in the proposed model.**

Parameters	Definitions	Value	Source
d	Birth/death rates	0.0011	[a]
α	Effective transmission rate of subclinical infection	variable	[b]
β	Effective transmission rate of clinical infection	variable	[b]
$1/\eta$	Duration of incubation period	4 days	[16]
$1/\delta$	Time span of humans from preclinical onset to clinical patients	1.5 days	[16]
$1/\omega$	Duration of treatment and recovery for clinical patients	14 days	[16]
$1/\gamma$	Duration of recovery for subclinical infectious	5 days	[16]
ϕ	The probability of exposed individuals progress to preclinical infectious	0.82	[16]
κ	Relative coefficient of migration matrix	variable	[b]
[a] It is estimated from the data in China's National Bureau of Statistics in 2019.			
[b] These parameters are estimated by MCMC method in this study.			

3 Basic reproduction number

The basic reproduction number R_0, as one of the most important theoretical concepts in epidemiology, acts the critical measure of the transmissibility [20]. R_0 is interpreted as the average

number of secondary cases that are produced by a single primary case in a fully susceptible population. In what follows, it is written $\mathbf{S} = (S_1, S_2, \ldots, S_n)^T$ and similarly for $\mathbf{E}, \mathbf{I^p}, \mathbf{I^s}, \mathbf{I^c}, \mathbf{R}$ and $\mathbf{N}$. The matrices

$$A_p = \begin{pmatrix} P_{11} & \cdots & P_{1n} \\ \vdots & \ddots & \vdots \\ P_{n1} & \cdots & P_{nn} \end{pmatrix} \begin{pmatrix} \lambda_1 \frac{P_1^T}{P_1^T \mathbf{N}} \\ \lambda_2 \frac{P_2^T}{P_2^T \mathbf{N}} \\ \vdots \\ \lambda_n \frac{P_n^T}{P_n^T \mathbf{N}} \end{pmatrix}$$

and the column vector P_i is the ith column of matrix $(P_{ij})_{n\times n}$. System (1) can then be written as the following vectorial notation:

$$\begin{cases} \dfrac{d\mathbf{S}}{dt} = d\mathbf{N} - \operatorname{diag}(\mathbf{S}) \left(A_p \mathbf{I^p} + \alpha A_p \mathbf{I^s} + \beta A_p \mathbf{I^c}\right) - d\mathbf{S}, \\ \dfrac{d\mathbf{E}}{dt} = \operatorname{diag}(\mathbf{S}) \left(A_p \mathbf{I^p} + \alpha A_p \mathbf{I^s} + \beta A_p \mathbf{I^c}\right) - (\eta + d)\, \mathbf{E}, \\ \dfrac{d\mathbf{I^p}}{dt} = \phi\eta \mathbf{E} - (\delta + d)\, \mathbf{I^p}, \\ \dfrac{d\mathbf{I^s}}{dt} = (1-\phi)\, \eta \mathbf{E} - (\gamma + d)\, \mathbf{I^s}, \\ \dfrac{d\mathbf{I^c}}{dt} = \delta \mathbf{I^p} - (\omega + d)\, \mathbf{I^c} \\ \dfrac{d\mathbf{R}}{dt} = \gamma \mathbf{I^s} + \omega \mathbf{I^c} - d\mathbf{R}. \end{cases} \tag{2}$$

Here for $u \in R^n$, $\operatorname{diag}(u)$ denotes the $n \times n$ diagonal matrix whose main diagonal is u. It is clear that

$$\Omega = \left\{(\mathbf{S}, \mathbf{E}, \mathbf{I^p}, \mathbf{I^s}, \mathbf{I^c}, \mathbf{R}) \in R_+^{6n} | 0 \le \mathbf{S}, \mathbf{E}, \mathbf{I^p}, \mathbf{I^s}, \mathbf{I^c}, \mathbf{R} \le \mathbf{N}\right\}$$

is a compact absorbing and positively invariant set for (2). Direct calculation yields that system (2) has a disease-free equilibrium, denoted as $Q_0 = \left(\mathbf{S^0}, \mathbf{E^0}, \mathbf{I^{p0}}, \mathbf{I^{s0}}, \mathbf{I^{c0}}, \mathbf{R^0}\right) = (\mathbf{N}, \mathbf{0}, \mathbf{0}, \mathbf{0}, \mathbf{0}, \mathbf{0})$.

The basic reproduction number R_0 is calculated by using the theory of next generation matrix [20]. It is written as $R_0 = \rho(FV^{-1})$, where F is the rate of occurring new infections, and V is the rate of transferring individuals outside the original group [20]. Here ρ represents the spectral radius of matrix. Based on the model (1), direct calculation yields that

$$F = \begin{pmatrix} \mathbf{0} & diag\mathbf{N}A_p & \alpha diag\mathbf{N}A_p & \beta diag\mathbf{N}A_p \\ \mathbf{0} & \mathbf{0} & \mathbf{0} & \mathbf{0} \\ \mathbf{0} & \mathbf{0} & \mathbf{0} & \mathbf{0} \\ \mathbf{0} & \mathbf{0} & \mathbf{0} & \mathbf{0} \end{pmatrix},$$

and

$$V = \begin{pmatrix} (\eta + d)\, \mathbf{I} & \mathbf{0} & \mathbf{0} & \mathbf{0} \\ -\phi\eta \mathbf{I} & (\delta + d)\, \mathbf{I} & \mathbf{0} & \mathbf{0} \\ -(1-\phi)\, \eta \mathbf{I} & \mathbf{0} & (\gamma + d)\, \mathbf{I} & \mathbf{0} \\ \mathbf{0} & -\delta \mathbf{I} & \mathbf{0} & (\omega + d)\, \mathbf{I} \end{pmatrix}.$$

where $\mathbf{I}$ denote a identity matrix, and $\mathbf{0}$ is the zero matrix. It follows from the characteristic equation of FV^{-1} that the basic reproduction number is given by

$$R_0 = \rho\left(\left(\frac{\phi\eta}{(\eta + d)\,(\delta + d)} + \frac{(1-\phi)\,\eta\alpha}{(\eta + d)\,(\gamma + d)} + \frac{\phi\eta\delta\beta}{(\eta + d)\,(\delta + d)\,(\omega + d)}\right) diag\mathbf{N}A_p\right). \tag{3}$$

The three components of the R_0 are separately contributed by the infections preclinical, subclinical, and clinical states.

4 Global stability

The results concerning the global dynamics of system (2) is analyzed in the following.

Theorem 4.1. *System (2) has a unique endemic equilibrium Q^*.*

Proof. It is denoted the expression of endemic equilibrium by $\mathbf{S}^*, \mathbf{E}^*, \mathbf{I^{p*}}, \mathbf{I^{s*}}$ and $\mathbf{I^{c*}}$. Based on the equilibrium definition, letting the right-hand side of system (2) to be zeros and substituting $\mathbf{S}^*, \mathbf{E}^*, \mathbf{I^{s*}}$ and $\mathbf{I^{c*}}$ by $\mathbf{I^{p*}}$, it is obtained an equation about $\mathbf{I^{p*}}$ as

$$f\left(\mathbf{I^{p*}}\right) = m_1 \mathbf{I^{p*}} diag(m_2 A_p \mathbf{I^{p*}})^{-1} \left(d\mathbf{I} + m_2 A_p \mathbf{I^{p*}}\right) - d\mathbf{N},$$

where

$$m_1 = \frac{(\eta + d)(\delta + d)}{\phi\eta}, m_2 = 1 + \frac{\alpha(1-\phi)(\delta+d)}{\phi(\gamma+d)} + \frac{\beta\delta}{\omega + d}.$$

Substituting $\mathbf{I^{p*}}$ by $\mathbf{0}$ and $\mathbf{N}$ yields that $f(\mathbf{0}) = -d\mathbf{N} < \mathbf{0}$, and

$$\begin{aligned} f(\mathbf{N}) &= m_1 \mathbf{N} diag(m_2 A_p \mathbf{N})^{-1} \left[d\mathbf{1} + m_2 A_p \mathbf{N}\right] - d\mathbf{N} \\ &\geq \tfrac{(\delta+d)}{\phi} \mathbf{N} diag(A_p \mathbf{N})^{-1} (A_p \mathbf{N}) - d\mathbf{N} = \tfrac{(\delta+d)}{\phi}\mathbf{N} - d\mathbf{N} > \mathbf{0}. \end{aligned}$$

It follows from the zero-point theorem that system (2) has at least one positive equilibrium. Furthermore, due to $f'(\mathbf{I^p}) = m_1 \mathbf{1} > \mathbf{0}$, f is an increasing function. Hence there exists a unique positive endemic equilibrium in the compact set Ω. □

Theorem 4.2. *If $R_0 < 1$, the disease-free equilibrium Q_0 of system (2) is globally asymptotically stable.*

Proof. Since the total number of human population is a constant, the first equation of system (2) can be ignored. Substituting $\mathbf{S}$ by $(\mathbf{N} - \mathbf{E} - \mathbf{I^p} - \mathbf{I^s} - \mathbf{I^c} - \mathbf{R})$, it is obtained

$$\begin{aligned} \frac{d\mathbf{E}}{dt} &= \mathrm{diag}\left(\mathbf{N} - \mathbf{E} - \mathbf{I^p} - \mathbf{I^s} - \mathbf{I^c} - \mathbf{R}\right)\left(A_p \mathbf{I^p} + \alpha A_p \mathbf{I^s} + \beta A_p \mathbf{I^c}\right) - (\eta + d)\,\mathbf{E} \\ &\leq \mathrm{diag}(\mathbf{N})\left(A_p \mathbf{I^p} + \alpha A_p \mathbf{I^s} + \beta A_p \mathbf{I^c}\right) - (\eta + d)\,\mathbf{E}. \end{aligned}$$

The corresponding comparison system is

$$\begin{cases} \dfrac{d\bar{\mathbf{E}}}{dt} = \mathrm{diag}(\mathbf{N})\left(A_p \bar{\mathbf{I}}^{\mathbf{p}} + \alpha A_p \bar{\mathbf{I}}^{\mathbf{s}} + \beta A_p \bar{\mathbf{I}}^{\mathbf{c}}\right) - (\eta + d)\,\bar{\mathbf{E}}, \\ \dfrac{d\bar{\mathbf{I}}^{\mathbf{p}}}{dt} = \phi\eta\bar{\mathbf{E}} - (\delta + d)\,\bar{\mathbf{I}}^{\mathbf{p}}, \\ \dfrac{d\bar{\mathbf{I}}^{\mathbf{s}}}{dt} = (1-\phi)\,\eta\bar{\mathbf{E}} - (\gamma + d)\,\bar{\mathbf{I}}^{\mathbf{s}}, \\ \dfrac{d\bar{\mathbf{I}}^{\mathbf{c}}}{dt} = \delta\bar{\mathbf{I}}^{\mathbf{p}} - (\omega + d)\,\bar{\mathbf{I}}^{\mathbf{c}}. \end{cases} \tag{4}$$

It is clear that model (4) is a linear system, and the coefficient matrix of its variables in the right-hand side is exactly the matrix $(F - V)$. Hence, when $R_0 = \rho\left(FV^{-1}\right) < 1$, the unique equilibrium $(\mathbf{E}, \mathbf{I^p}, \mathbf{I^s}, \mathbf{I^c}) = (\mathbf{0}, \mathbf{0}, \mathbf{0}, \mathbf{0})$ of this linear system (4) is globally asymptotically stable. Since

$$\frac{d\mathbf{E}}{dt} \leq \frac{d\bar{\mathbf{E}}}{dt}, \frac{d\mathbf{I^p}}{dt} \leq \frac{d\bar{\mathbf{I}}^{\mathbf{p}}}{dt}, \frac{d\mathbf{I^s}}{dt} \leq \frac{d\bar{\mathbf{I}}^{\mathbf{s}}}{dt}, \frac{d\mathbf{I^c}}{dt} \leq \frac{d\bar{\mathbf{I}}^{\mathbf{c}}}{dt}.$$

According to the comparison theorem, with the same initial conditions, it has $\mathbf{E(t)} \leq \bar{\mathbf{E}}\mathbf{(t)}$, $\mathbf{I^p(t)} \leq \bar{\mathbf{I}}^{\mathbf{p}}\mathbf{(t)}$, $\mathbf{I^s(t)} \leq \bar{\mathbf{I}}^{\mathbf{s}}\mathbf{(t)}$, and $\mathbf{I^c(t)} \leq \bar{\mathbf{I}}^{\mathbf{c}}\mathbf{(t)}$ for any $t > 0$, yielding that Q_0 is globally asymptotically stable when $R_0 < 1$. □

To establish global stability results of the endemic equilibrium, it is used the graph-theoretic method as presented in [21] and [22].

Theorem 4.3. *If $R_0 > 1$, then, the unique endemic equilibrium Q^* of system (2) is globally asymptotically stable in Ω.*

Proof. Denote

$$D_i = S_i - S_i^* - S_i^* \ln \frac{S_i}{S_i^*} + E_i - E_i^* - E_i^* \ln \frac{E_i}{E_i^*}, D_{n+i} = I_i^p - I_i^{p*} - I_i^{p*} \ln \frac{I_i^p}{I_i^{p*}},$$

$$D_{2n+i} = I_i^s - I_i^{s*} - I_i^{s*} \ln \frac{I_i^s}{I_i^{s*}}, D_{3n+i} = I_i^c - I_i^{c*} - I_i^{c*} \ln \frac{I_i^c}{I_i^{c*}}, \tilde{N}_j = \sum_{k=1}^{n} P_{kj} N_k,$$

where the variable with superscript as star are the expressions of endemic equilibrium in the model. Using the inequality $1 - x + \ln x \leq 0$, for $x > 0$, direct differentiation yields:

$$\begin{aligned}
D_i{}' &= \sum_{j=1}^{n} \lambda_j P_{ij} S_i^* {\ell_j}^* + dS_i^* - \sum_{j=1}^{n} \lambda_j P_{ij} S_i \ell_j - dS_i - \sum_{j=1}^{n} \lambda_j P_{ij} S_i^* \frac{S_i^*}{S_i} {\ell_j}^* - d\frac{S_i^* S_i^*}{S_i} + \sum_{j=1}^{n} \lambda_j P_{ij} S_i^* \ell_j + dS_i^* \\
&+ \sum_{j=1}^{n} \lambda_j P_{ij} S_i \ell_j - \sum_{j=1}^{n} \lambda_j P_{ij} S_i^* \frac{E_i}{E_i^*} {\ell_j}^* - \sum_{j=1}^{n} \lambda_j P_{ij} S_i \frac{E_i^*}{E_i} \ell_j + \sum_{j=1}^{n} \lambda_j P_{ij} S_i^* {\ell_j}^* \\
&\leq \sum_{j=1}^{n} \lambda_j P_{ij} S_i^* {\ell_j}^* - \sum_{j=1}^{n} \lambda_j P_{ij} S_i \ell_j - \sum_{j=1}^{n} \lambda_j P_{ij} S_i^* \frac{S_i^*}{S_i} {\ell_j}^* + \sum_{j=1}^{n} \lambda_j P_{ij} S_i^* \ell_j \\
&+ \sum_{j=1}^{n} \lambda_j P_{ij} S_i - \sum_{j=1}^{n} \lambda_j P_{ij} S_i^* \frac{E_i}{E_i^*} {\ell_j}^* - \sum_{j=1}^{n} \lambda_j P_{ij} S_i \frac{E_i^*}{E_i} \ell_j + \sum_{j=1}^{n} \lambda_j P_{ij} S_i^* {\ell_j}^* \\
&= \sum_{j=1}^{n} \lambda_j P_{ij} S_i^* \varpi_j^p \left(1 - \frac{S_i I_k^p}{S_i^* I_k^{p*}} - \frac{S_i^*}{S_i} + \frac{I_k^p}{I_k^{p*}}\right) + \sum_{j=1}^{n} \lambda_j P_{ij} S_i^* \alpha \varpi_j^s \left(1 - \frac{S_i I_k^s}{S_i^* I_k^{s*}} - \frac{S_i^*}{S_i} + \frac{I_k^s}{I_k^{s*}}\right) \\
&+ \sum_{j=1}^{n} \lambda_j P_{ij} S_i^* \beta \varpi_j^c \left(1 - \frac{S_i I_k^c}{S_i^* I_k^{c*}} - \frac{S_i^*}{S_i} + \frac{I_k^c}{I_k^{c*}}\right) + \sum_{j=1}^{n} \lambda_j P_{ij} S_i^* \varpi_j^p \left(1 + \frac{S_i I_k^p}{S_i^* I_k^{p*}} - \frac{E_i}{E_i^*} - \frac{E_i^* S_i I_k^p}{E_i S_i^* I_k^{p*}}\right) \\
&+ \sum_{j=1}^{n} \lambda_j P_{ij} S_i^* \alpha \varpi_j^s \left(1 + \frac{S_i I_k^s}{S_i^* I_k^{s*}} - \frac{E_i}{E_i^*} - \frac{E_i^* S_i I_k^s}{E_i S_i^* I_k^{s*}}\right) + \sum_{j=1}^{n} \lambda_j P_{ij} S_i^* \beta \varpi_j^c \left(1 + \frac{S_i I_k^c}{S_i^* I_k^{c*}} - \frac{E_i}{E_i^*} - \frac{E_i^* S_i I_k^c}{E_i S_i^* I_k^{c*}}\right) \\
&\leq \sum_{j=1}^{n} \lambda_j P_{ij} S_i^* \varpi_j^p \left(\frac{I_k^p}{I_k^{p*}} - \ln \frac{I_k^p}{I_k^{p*}} + \ln \frac{E_i}{E_i^*} - \frac{E_i}{E_i^*}\right) + \sum_{j=1}^{n} \lambda_j P_{ij} S_i^* \alpha \varpi_j^s \left(\frac{I_k^s}{I_k^{s*}} - \ln \frac{I_k^s}{I_k^{s*}} + \ln \frac{E_i}{E_i^*} - \frac{E_i}{E_i^*}\right) \\
&+ \sum_{j=1}^{n} \lambda_j P_{ij} S_i^* \beta \varpi_j^c \left(\frac{I_k^c}{I_k^{c*}} - \ln \frac{I_k^c}{I_k^{c*}} + \ln \frac{E_i}{E_i^*} - \frac{E_i}{E_i^*}\right) \\
&=: a_{i,n+i} G_{i,n+i} + a_{i,2n+i} G_{i,2n+i} + a_{i,3n+i} G_{i,3n+i}.
\end{aligned}$$

Here,

$${\ell_j}^* = \frac{1}{\tilde{N}_j} \sum_{k=1}^{n} P_{kj} \left(I_k^{p*} + \alpha I_k^{s*} + \beta I_k^{c*}\right), \ell_j = \frac{1}{\tilde{N}_j} \sum_{k=1}^{n} P_{kj} \left(I_k^p + \alpha I_k^s + \beta I_k^c\right),$$

$$\varpi_j^p = \frac{1}{\tilde{N}_j} \sum_{k=1}^{n} P_{kj} I_k^{p*}, \ \varpi_j^s = \frac{1}{\tilde{N}_j} \sum_{k=1}^{n} P_{kj} I_k^{s*}, \ \varpi_j^c = \frac{1}{\tilde{N}_j} \sum_{k=1}^{n} P_{kj} I_k^{c*}.$$

Similarly,

$$\begin{aligned}
D'_{n+i} &= \phi\eta E_i - \phi\eta E_i^* \frac{I_i^p}{I_i^{p*}} - \phi\eta E_i \frac{I_i^{p*}}{I_i^p} + \phi\eta E_i^* = \phi\eta E_i^* \left(1 - \frac{E_i I_i^{p*}}{E_i^* I_i^p} - \frac{I_i^p}{I_i^{p*}} + \frac{E_i}{E_i^*}\right) \\
&\leq \phi\eta E_i^* \left(\frac{E_i}{E_i^*} - \ln \frac{E_i}{E_i^*} + \ln \frac{I_i^p}{I_i^{p*}} - \frac{I_i^p}{I_i^{p*}}\right) =: a_{n+i,i} G_{n+i,i}.
\end{aligned}$$

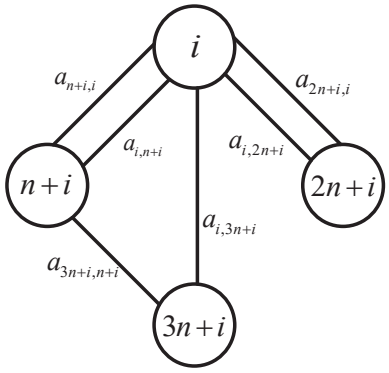

Figure 2: Digraph representation of the matrix A of transmission used to determine the coefficients in the Lyapunov function D.

$$
\begin{aligned}
D'_{2n+i} &= (1-\phi)\,\eta E_i - (1-\phi)\,\eta E_i^* \tfrac{I_i^s}{I_i^{s*}} - (1-\phi)\,\eta E_i \tfrac{I_i^{s*}}{I_i^s} + (1-\phi)\,\eta E_i^* \\
&= (1-\phi)\,\eta E_i^* \left(1 - \tfrac{E_i I_i^{s*}}{E_i^* I_i^s} - \tfrac{I_i^s}{I_i^{s*}} + \tfrac{E_i}{E_i^*}\right) \\
&\le (1-\phi)\,\eta E_i^* \left(\tfrac{E_i}{E_i^*} - \ln \tfrac{E_i}{E_i^*} + \ln \tfrac{I_i^s}{I_i^{s*}} - \tfrac{I_i^s}{I_i^{s*}}\right) =: a_{2n+i,i} G_{2n+i,i}. \\
D'_{3n+i} &= \delta I_i^p - \delta I_i^{p*} \tfrac{I_i^c}{I_i^{c*}} - \delta I_i^p \tfrac{I_i^{s*}}{I_i^s} + \delta I_i^{p*} = \delta I_i^{p*} \left(1 - \tfrac{I_i^p I_i^{c*}}{I_i^{p*} I_i^c} - \tfrac{I_i^c}{I_i^{c*}} + \tfrac{I_i^p}{I_i^{p*}}\right) \\
&\le \delta I_i^{p*} \left(\tfrac{I_i^p}{I_i^{p*}} - \ln \tfrac{I_i^p}{I_i^{p*}} + \ln \tfrac{I_i^c}{I_i^{c*}} - \tfrac{I_i^c}{I_i^{c*}}\right) =: a_{3n+i,n+i} G_{3n+i,n+i}.
\end{aligned}
$$

and

$$
a_{i,n+i} = \frac{\lambda_j P_{ij} S_i^*}{\tilde{N}_j} \sum_{k=1}^n P_{kj} I_k^{p*},\ a_{i,2n+i} = \frac{\lambda_j P_{ij} S_i^* \alpha}{\tilde{N}_j} \sum_{k=1}^n P_{kj} I_k^{s*},\ a_{i,3n+i} = \frac{\lambda_j P_{ij} S_i^* \beta}{\tilde{N}_j} \sum_{k=1}^n P_{kj} I_k^{c*},
$$

as well as $a_{n+i,i} = \phi\eta E_i^*, a_{2n+i,i} = (1-\phi)\,\eta E_i^*, a_{3n+i,i} = \delta I_i^{p*}$. Let $A = (a_{ij})_{n\times n}$ with $a_{ij} > 0$ as defined above and otherwise zero. The corresponding weighted digraph is shown in Figure 2. Along each of the cycles on the graph, it is verified that $\sum G_{ij} = 0$; for instance, $G_{i,n+i} + G_{n+i,i} = 0, G_{j,n+i} + G_{n+j,j} + G_{i,n+j} + G_{n+i,i} = 0$, and so on. It follows from Theorem 3.5 in [21] that there exist constants c_i such that $D = \sum_i c_i Q_i$ is a Lyapunov function for system (2). Let $c_1 = \cdots = c_n = 1$, and

$$
c_{n+i} = \sum_{j=1}^n \frac{(c_j a_{j,n+i} + c_j a_{j,3n+i})}{a_{n+i,i}},\ c_{2n+i} = \sum_{j=1}^n \frac{c_j a_{j,2n+i}}{a_{2n+i,i}},\ c_{3n+i} = \sum_{j=1}^n \frac{c_j a_{j,3n+i}}{a_{3n+i,n+i}}.
$$

Further computation leads to

$$
\begin{aligned}
c_{n+i} &= \sum_{j=1}^n \left[\tfrac{\lambda_j P_{ij} S_i^*}{\tilde{N}_j \phi\eta E_i^*} \left(\sum_{k=1}^n P_{kj} I_k^{p*} + \beta \sum_{k=1}^n P_{kj} I_k^{c*}\right)\right], \\
c_{2n+i} &= \sum_{j=1}^n \left(\tfrac{\lambda_j P_{ij} S_i^* \alpha}{(1-\phi)\eta E_i^* \tilde{N}_j} \sum_{k=1}^n P_{kj} I_k^{s*}\right),\ c_{3n+i} = \sum_{j=1}^n \left(\tfrac{\lambda_j P_{ij} S_i^* \beta}{\delta I_i^{p*} \tilde{N}_j} \sum_{k=1}^n P_{kj} I_k^{c*}\right).
\end{aligned}
$$

Hence, with the functions D_i and constants c_i given above, the expression

$$
D = \sum_{i=1}^n c_i D_i + \sum_{i=1}^n c_{n+i} D_{n+i} + \sum_{i=1}^n c_{2n+i} D_{2n+i} + \sum_{i=1}^n c_{3n+i} D_{3n+i}
$$

is a Lyapunov function for system (2). Its derivative is

$$\begin{aligned} D' &= \sum_{i=1}^{n} c_i \left(\frac{S_i - S_i^*}{S_i} S_i{}' + \frac{E_i - E_i^*}{E_i} E_i{}' \right) + \sum_{i=1}^{n} c_{n+i} \left(\frac{I_i^p - I_i^{p*}}{I_i^p} I_i^{p\prime} \right) \\ &+ \sum_{i=1}^{n} c_{2n+i} \left(\frac{I_i^s - I_i^{s*}}{I_i^s} I_i^{s\prime} \right) + \sum_{i=1}^{n} c_{3n+i} \left(\frac{I_i^c - I_i^{c*}}{I_i^c} I_i^{c\prime} \right). \end{aligned}$$

When $D' = 0$ in the set $\left\{R_+^{5n}\right\}$, one can readily verify that $S_i = S_i^*, E_i = E_i^*, I_i^p = I_i^{p*}, I_i^s = I_i^{s*}, I_i^c = I_i^{c*}$. For the left system,

$$\frac{dR_i}{dt} = \gamma I_i^{s*} + \omega I_i^{c*} - dR_i. \tag{5}$$

it is clear that system () has a unique equilibrium $R_i = R_i^*$, which is global asymptotically stable. Using LaSalle's Invariance Principle, it is concluded that the endemic equilibrium Q^* is global asymptotically stable in Ω.

□

5 Application to the outbreak in China

In this section, the proposed model is applied to analyze the spatiotemporal transmission dynamics of COVID-19 in Chinese provinces. Daily records of human infections were collected from authoritative data report. The permanent population size in each province were released by the 2019 National Bureau of Statistics. The daily migration data among provinces is collected from Baidu migration data (https://qianxi.baidu.com/).

The model is validated by using Markov chain Monte Carlo (MCMC) method to fit the daily reported cases in 26 provinces (with cases more than 101 from 5 January 2020 to 15 March 2020). Here 6 parameters (β, α, κ, and the initial values of E, I^c and I^p in HuB) were estimated by MCMC. Since HuB province is considered to be the infection source, it is assumed that there is no infections in other provinces at initial time. The transmission rate λ_i is derived from the effective reproduction number R_t in province i. R_t represents the number of new morbidity cases caused by an average morbidity case at time t. Here the R_t in each province is estimated from the time series of its indigenous cases. Based on Bayesian framework, R_t is calculated by the EpiEstim package in R language software [23], in which the intergenerational time follows gamma distribution, with the mean value and standard deviation as 7.5 and 3.4 respectively [24].

The fitting results are shown in Figures 3 and S1 (in Supplementary Information). It is found that the model performed well in fitting the daily reported incidences, except the data in some provinces such as HeB, ZJ, HeN, HuN, CQ and GZ. The fitting deviations are possibly due to the spatiotemporal heterogeneity of transmission parameters and detection efficiency. PRCC coefficients are used as global sensitivity to quantify the response of model outputs to the variation of the estimated parameters. By averaging the daily PRCC coefficients in the operation of fitting daily incidences, it is found that the output is strongly sensitive to the effective transmission rate of clinical infection (β) and the relative coefficient of migration matrix (κ), followed by the effective transmission rate of subclinical infection (α). Yet it seems that in the entire infection process the output is scarcely sensitive to the initial condition of the model. The reason for the negative correlation of β and κ with model output is that for given R_t, small values of β and κ mean large values of transmission rates λ.

In the following simulations of the model, it is set that (1) the initial conditions are $E(0) = 50, I^p(0) = I^s(0) = I^c(0) = 35$ in Figures 4, 5 and S6, and $E(0) = I^p(0) = I^s(0) = I^c(0) = 20$ in Figures 6 and 7; (2) the impact of human mobility is reflected by the migration matrix P, and its values are selected from Baidu migration data during 2020 and 2021; and (3) multiple interventions (including social distancing, quarantine and wearing masks, etc.) are measured by different values of the effective reproduction number R_t, in which the largest and minimum values are separately $R_t = 3.56$ and $R_t = 0.59$, corresponding to the situations of no intervention (in early infection

Table 2: **Province and its abbreviation in China**

Province	Hubei	Beijing	tianjin	Hebei	Shanxi	Liaoning	Jilin	Heilongjiang
Abbreviation	HuB	BJ	TJ	HeB	SX	LN	JL	HLJ
Province	Shanghai	Jiangsu	Zhejiang	Anhui	Fujian	Jiangxi	Shandong	Henan
Abbreviation	SH	JS	ZJ	AH	FJ	JX	SD	HeN
Province	Hunan	Guangdong	Guangxi	Hainan	Chongqing	Sichuan	Guizhou	Yunnan
Abbreviation	HuN	GD	GX	HaiN	CQ	SC	GZ	YN
Province	Shaanxi	Gansu	Qinghai	Ningxia	Xinjiang	Neimenggu	Xizang	
Abbreviation	SaX	GS	QH	NX	XJ	NMG	XZ	

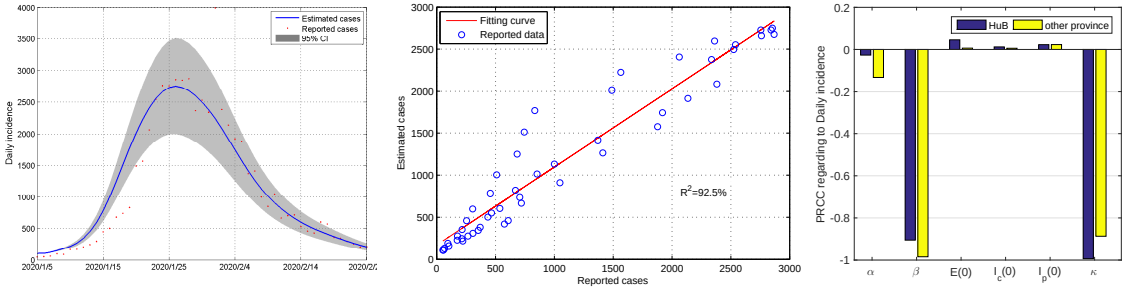

(a) (b) (c)

Figure 3: The fitting results of the COVID-19 cases in China. (a) Fitting daily new cases in HuB, where the light shaded area is the 95% confidence interval (CI) for all 1000 simulations, and the blue curve is the median of the model output; (b) Relationship between predicted and observed cases in HuB. (a) Sensitivity of daily cases to the model parameters as indicated by PRCC values.

stage [2020.1.5-2020.1.22] in HuB) and rigorous intervention (in the mid to late stage of infection [2020.1.23-2020.2.12] in HuB).

Figure 4 show the impacts of intervention on the evolution of COVID-19 in China, with different initial infection site (i.e., HuB, BJ, SH, GD and XZ). The migration data during 23 January 2021 and 20 March 2021 are integrated into the model for simulating the transmission process under two modes: few intervention and rigorous intervention. These two modes are reflected by the choices of the reproduction number, whose values in each province are taken as the means of the effective reproduction number at the beginning of the outbreak (2020.1.5-2020.1.22) and after the intervention (2020.1.23-2020.2.12), respectively. For simulating the transmission for 57 days, the following patterns are observed in Figure 4. First, in case of substituting the early R_t into the model, the infection burden could increase hundreds of times, in which the numbers of total infections in China could reach 111.08, 64.61, 66.71, 57.62 and 13.59 million with separate source of initial infection in HuB, BJ, SH, GD and XZ. Second, in case of substituting the latter R_t into the model, the above numbers reduce sharply to 228, 288, 215, 232 and 154. Moreover, the regions around source of initial infection would likely suffer more serious attack, in which the highest attack rates are: 0.28 in HuB and 0.14 in GZ with source in HuB, 0.20 in TJ and 0.12 in HuB with source in BJ, 0.10 in JS and 0.09 in AN with source in SH, 0.15 in GZ and 0.09 in HuB with source in GD, 0.19 in XZ and 0.1 in QH with source in XZ.

Figure 5 shows the ranking of total infections in China with a unique infection source at initial time and human mobility at the entire process. Here it is assumed that there is no implementation of intervention, which is realized by setting the reproduction number in each province to be the value in early infection stage in HuB (equal 3.56). By simulating the transmission process through 57 days, it is found that (1) the initial infection located in HeN, ZJ, SH, JS and AH would caused the top five numbers of human cases (over 300 million); (2) when the initial infection is located in XZ, QH, JL, HLJ, XJ, it would lead to smallest infection sizes (around 142-183 million). Moreover, by simulating the transmission process through 120 days, it is observed that the infection would reach a saturated state: more than 1.1 billion people could be infected no matter where the infection initially occurs. In this case, all provinces reach the highest levels of new infections after about

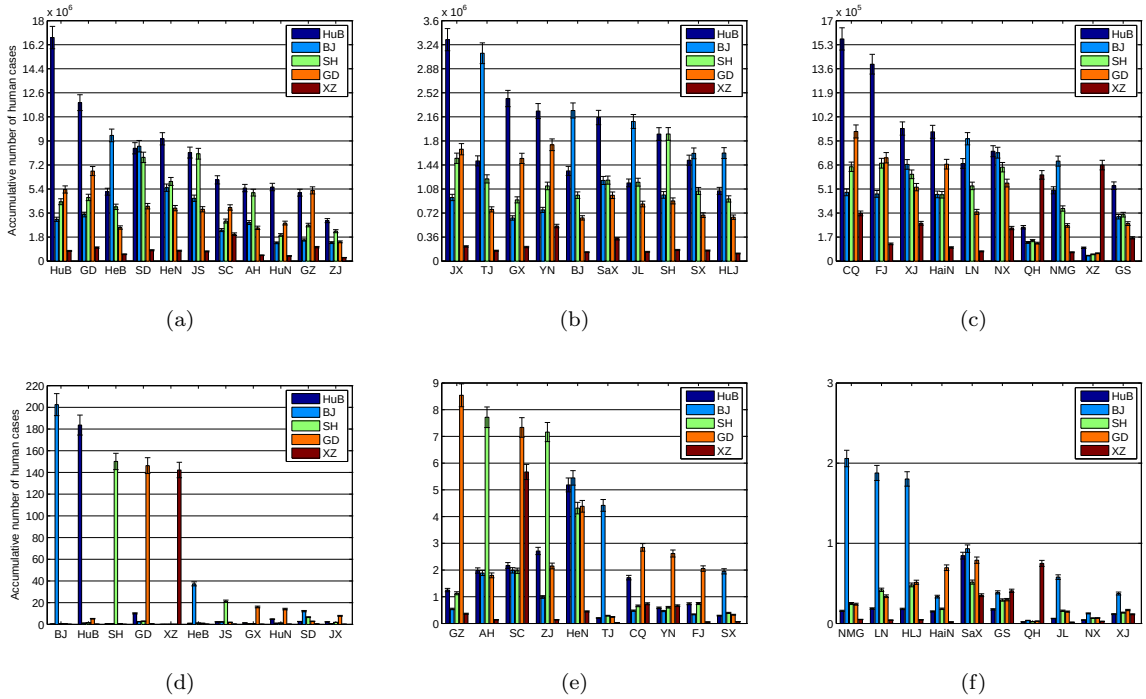

Figure 4: The accumulative number of cases in each province before and after the intervention, in case of different locations (HuB, BJ, SH, GD, XZ) of initial infection. The human mobility information is adopted from the data during 23 January 2021 and 20 March 2021. The transmission rate λ in Figures (a), (b), (c) and (d), (e), (f) are separately determined by the mean values of effective reproduction number before and after the intervention.

two months (see Figure S3), but the attack rate exhibits spatial heterogeneity, in which the area near the initial infection source usually suffers worse.

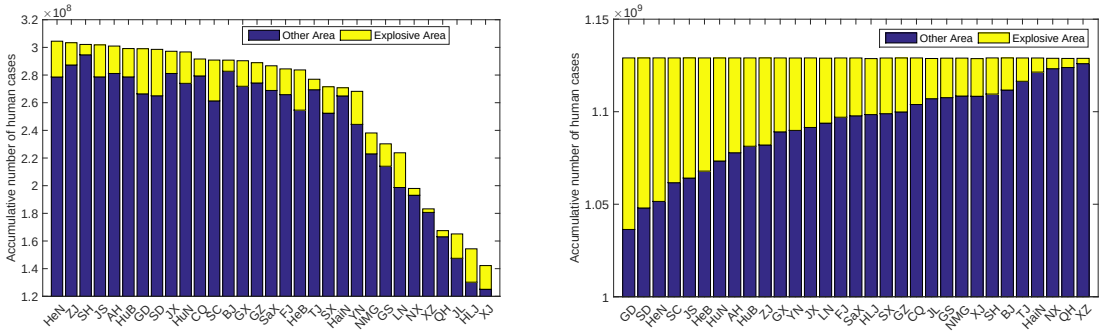

(a) (b)

Figure 5: The cumulative number of cases in China with the human mobility data (a) from January 23, 2021 to March 20, 2021, and (b) from January 23, 2021 to May 20, 2021, in case of no implementation of social distance. The abscissa is the location that has unique infection source at initial time. The yellow part is the contribution by the the location with initial infections.

Figure 6 shows the impacts of different conditions of initial infection and human mobility on the evolution of COVID-19 transmission among the provinces in China, in case of no intervention. It is observed that more sites with initial infection and more frequency of human mobility would yield a little faster diffusion of the disease (that is more obvious in early infection period) and a little earlier arriving of the peak. When the disease starts to spread from January 23, 2021, the numbers of human cases would reach peak around early April or late March, in case of one initial infection site(XZ), or two initial infection sites (HeN and GD). However, in case of all size with initial infection, the peak is arriving basically in the middle of March, regardless of population mobility. In these four settings, the infection would last for three months, causing similar number of total infections.

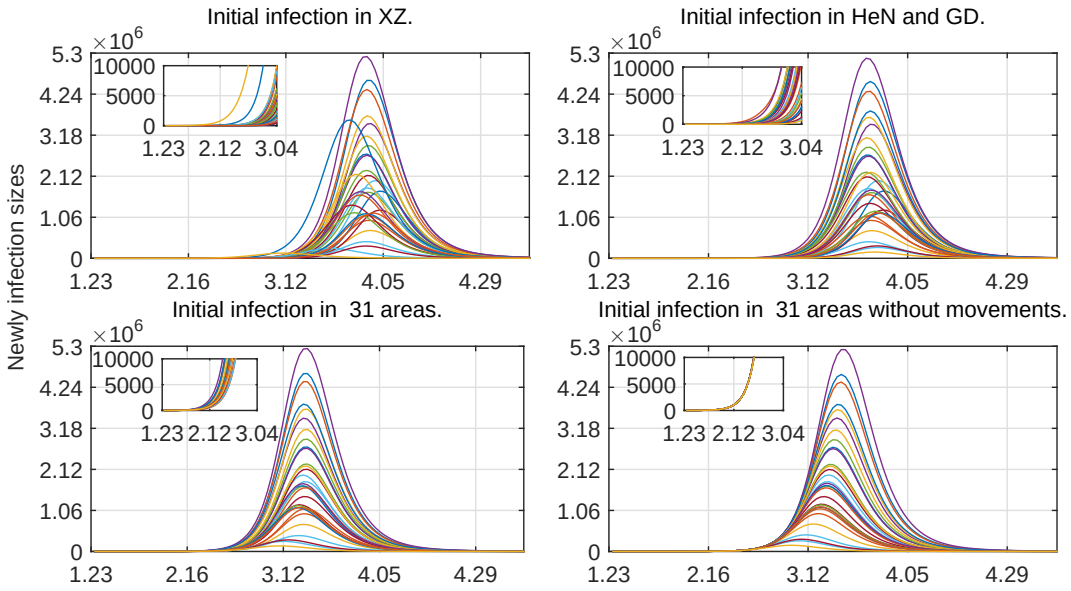

Figure 6: Time series of daily new cases in each province with different outbreak sites at initial time and human mobility data from January 23, 2021 to May 20, 2021, in case of no intervention.

Figure 7 shows the evolution dynamics of COVID-19 in China with different patterns of intervention, in case of only GD as the initial infection site. Here the impacts of intervention and human mobility are quantified by the basic reproduction number R_0 and travel ban, respectively. It is found that (1) slight increase of R_0 would cause rapid transmission and high morbidity around China, (2) travel ban among the provinces in China as early as possible can postpone the propagation a little bit and possibly reduce total morbidity, and (3) the control effect of travel ban is not significant (especially for large R_0), only when the travel is restricted at first. Specifically, (1) when $R_0 = 3.56, 2.5, 2, 1.5$, and 1.1, human infections increase rapidly after 14, 29, 56, 72, and 81 days since the introduction of the infection, respectively; (2) when $R_0 = 3.56, 2.5$, and 2, the number of infections would reach the peak around March 27, May 2, and Jun 7, resulting in total infections to be 1.1, 1.0, and 0.8 billion (regardless when to start travel ban after outbreak), but the numbers would reduce vastly to 92.8, 75.9 and 85.7 million if travel ban starts before outbreak; (3) when $R_0 = 2$, if travel ban is implemented after 1 day, 10 days and 20 days of the break, the transmission could be postponed 2 day, 5 day, and 18 days (compared with the case without travel ban), resulting in 735.5 million, 865.6 million and 876.21 million of human infections; and (4) in case of rigorous intervention ($R_0 < 1$), it is impossible for travel to trigger disease outbreak.

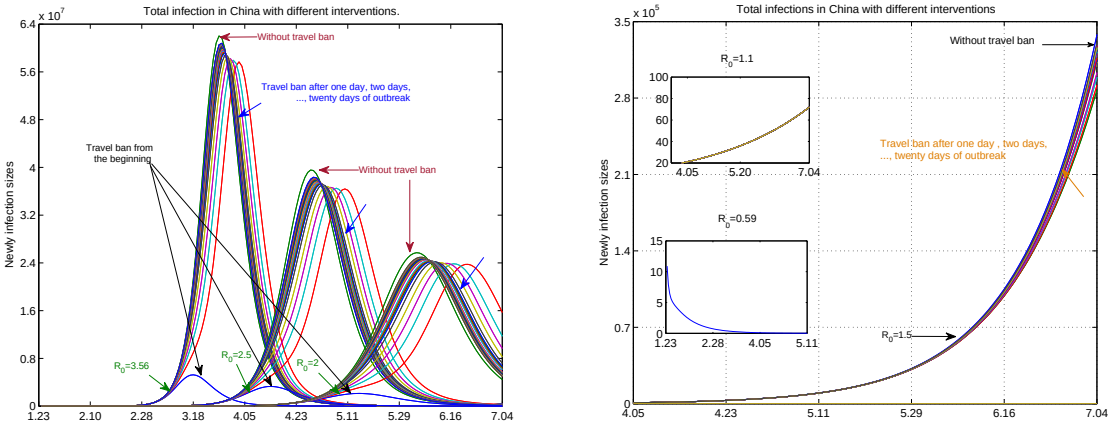

(a) (b)

Figure 7: Time series of daily new cases in China with different timing of travel ban and different basic reproduction number. Here human mobility information is selected from the data during January 23, 2021 and July 4, 2021.

6 Discussion

COVID-19 is posing increasing threats to public health around the world. Clear information about epidemiologic features and transmission patterns of the disease can help to control and prevent COVID-19 transmission. The present study is an attempt to provide a modeling framework to infer COVID-19 spatiotemporal transmission patterns by focusing on the COVID-19 outbreak in 31 provinces of China.

Since the outbreak of COVID-19, many epidemiological models have been proposed and applied to study the propagation of COVID-19. Focusing on the spatiotemporal transmission, modeling framework including mathematical model (e.g., ordinary/partial differential equation [9, 10, 11, 12, 15, 16, 19], difference equations [13],) computational model (e.g., agent-based model [17] and next-generation algorithm [18]), and statistical model (e.g., stochastic model [14] and ArcGIS [25]). Inspired by existing studies, this paper presented a new mathematical model via ODEs, which couples the intrinsic transmission dynamics, including the disease evolution in humans among different states (susceptible, exposed, preclinical infectious, subclinical infectious, clinical infectious

and recovered), infection action by human-human contact, and human mobility among different regions. Moreover, the effects of human behavior and control strategy were characterized by model parameters, which can regulate the the spatiotemporal infectivity and transmissibility. Finally, MCMC algorithm was employed to estimate the uncertain parameters and then to evaluate the model. The modeling framework is an update of recent studies. By validating the proposed model with surveillance data in 31 provinces of China, the spatiotemporal transmission dynamics and the effects of human mobility and interventions were clarified, which can providing the following clues for guiding disease control.

First, there is a unique epidemic threshold, denoted by basic reproduction number R_0, which can totally determine whether COVID-19 proceeds among multiple regions. If $R_0 < 1$, no matter how many infection sources there are, COVID-19 will always die out. Otherwise, the disease will persist in each region. R_0 unites infectivity in each region by human mobility. Such mobility contributes to transmission in two ways: susceptible persons in other regions could be infected when traveling to outbreak area, and infected persons may bring COVID-19 virus from outbreak area to other regions. Particularly, when $R_0 > 1$, no region can escape from infection if there exists human mobility among them.

Second, the effects of the implemented intervention in China are further evaluated. By using the proposed model to simulate the spatiotemporal transmission dynamics, it is found that if the interventions (e.g., social distancing, city lockdown, etc.) had not been implemented in China, COVID-19 would prevail all around China and the transmission would last about three months, resulting in over 1.1 billion patients. In this case, more than 78.6% population in China would be infected by COVID-19 virus, which is over 11,981 times of the total number of reported cases. The estimated effects of interventions are much more significant than previous results, which claimed that (1) if without non-pharmaceutical interventions in China, the number of cases was predicted to be 7.6 million by 29 February 2020 [15], or 37 million by 5 March 2020 [26], or increase the total infections by 93.7% [27]. The reason for the severity of our estimation could be that this study highlights the intrinsic spatiotemporal transmission dynamics and the total infection process.

Third, the role of human mobility in COVID-19 transmission is further clarified. Similarly to previous studies [13, 25, 27], it is verified that human mobility (by travel) can spark new infections in virgin areas and high frequency of human mobility in reality has driven COVID-19 diffusion across the 31 provinces of China. The present paper further indicates that the effects of human mobility in the spatiotemporal transmission of COVID-19 is more prominent in two cases: early stage of infection and when R_0 is a little bigger than one. If without intervention inside region, then human mobility would accelerate disease propagation across different regions, but it could not modify the number of total infections, unless travel is banned at the very beginning of infection. Hence, regional human migration plays as a trigger in the preliminary stage of infection, and then locally contracted infection dominates the following transmission process. The results demonstrate that non-pharmaceutical intervention is the core strategy, and travel ban at the same time can slow down the process and suppress incidence rate.

Fourth, the transmission patterns of COVID-19 in the whole country are further inferred. The initial infection located in central and east of China (HeN, ZJ, SH, JS and AH) would easily stimulate quick outbreak and large infection, but adverse consequence is observed if initial infection is located in west and northeast of China (XJ, HLJ, QH, XZ, GS, NMG, and YN), in that there exists less population flow. Yet if without any intervention, the transmission would continue three months, and then no matter where the outbreak occurs and how many sits do initial infection locates, the infections of COVID-19 would reach a saturation level, and more than 87% people in China would be infected.

In view of current situation of COVID-19 pandemic, China is facing high risk of sporadic outbreaks due to imported infections and is making great efforts for prevention. To control this disease, beside promoting vaccination (that is precisely what China is doing), the present study suggests that (1) identifying and isolating imported case is the primary mission, which can be accomplished by monitoring the travellers from foreign countries by tight and thorough surveillance system; and (2) in case of autochthonous infection, strict non-pharmaceutical interventions must be taken as soon as possible, including tracking close contacts and quarantine, travel restriction,

lockdown of high risky community. Indeed, such intervention strategies are exactly as China is implementing. By doing so, more than 99.99% human infections would has been avoided according to this study.

Here several limitations need to be clarified. (1) The COVID-19 incidence data was based on public report information, which may yields data deviation from reality. (2) The biological parameters applied in the proposed model were extracted from literature, which may show geographical disparities. (3) The model did not take into account the potential factors such as the difference of immunity and infectivity. Nevertheless, the model captures the dynamic evolution of disease in time and place, and incorporated the biologically intuitive parameterizations. It matches well with spatiotemporal data by fitting several parameters, lending confidence to the analysis and justifying the model's further generalization.

In summary, this paper develops an inference technique to identify COVID-19 transmission patterns and it is applied to explore the COVID-19 transmission patterns in the provinces of China. The proposed model takes into account the essential effects of human mobility and disease evolution, which allow to capture the hidden spatiotemporal dynamics and internal mechanism of COVID-19 transmission. The obtained results support the interventions that are being implemented in China.

Authors contributions HL and GZ designed the study. QJ, JL, HL and FT collected the data. QJ, JL, HL and GZ built the model and performed the analysis. QJ, JL and FT interpreted the data. QJ and GZ prepared the manuscript. All authors reviewed and approved the submitted manuscript.

Acknowledgements This work was supported by the National Natural Science Foundation of China (82041021), and the Innovation Project of GUET Graduate Education (2021YCXS111 and 2020YCXS085).

Data availability The data that support the findings of this study is available from the corresponding author upon reasonable request.

Declaration

Conflicts of Interest: The authors declare no conflict of interest.

References

[1] World Health Organization (WHO). Coronavirus disease (COVID-19) pandemic. *https://www.who.int/zh/emergencies/diseases/novel-coronavirus-2019*.

[2] CDC. Epidemic update and risk assessment of 2019 Novel Coronavirus.

[3] Mukandavire Z Cuadros D F, Xiao Y et al. Spatiotemporal transmission dynamics of the COVID-19 pandemic and its impact on critical healthcare capacity. *Health and Place*, 64:102404, 2020.

[4] Ak C Masa B, Sk A et al. COVID-19 infection: Origin, transmission, and characteristics of human coronaviruses. *Journal of Advanced Research*, 24:91–98, 2020.

[5] Xc C Ming G A, Ly B et al. A study on infectivity of asymptomatic SARS-CoV-2 carriers-sciencedirect. *Respiratory Medicine*, 169:106026, 2020.

[6] Akhmetzhanov A R Nishiura H, Linton N M. Serial interval of novel coronavirus (COVID-19) infections. *International Journal of Infectious Diseases*, 93:284–286, 2020.

[7] Ko A I Pollitt K, Peccia J et al. COVID-19 vulnerability: The potential impact of genetic susceptibility and airborne transmission. *Human Genomics*, 14:1–7, 2020.

[8] Ferguson N M. Kamp C. Untangling the interplay between epidemic spread and transmission network dynamics. *Plos Computational Biology*, 6(11):e1000984, 2010.

[9] Sun K. He S, Peng Y. SEIR modeling of the COVID-19 and its dynamics. *Nonlinear Dynamics*, 101(3):1667–1680, 2020.

[10] Zhou Y Hou C, Chen J et al. The effectiveness of quarantine of Wuhan city against the Corona Virus Disease 2019 (COVID-19): A well-mixed SEIR model analysis. *Journal of Medical Virology*, 92(7):841–848, 2020.

[11] Wang K Yang Z, Zeng Z et al. Modified SEIR and AI prediction of the epidemics trend of COVID-19 in China under public health interventions. *Journal of Thoracic Disease*, 12(3):165–174, 2020.

[12] Auricchio F Viguerie A, Lorenzo G et al. Simulating the spread of COVID-19 via spatially-resolved susceptible-exposed-infected-recovered-deceased (SEIRD) model with heterogeneous diffusion. *Applied Mathematics Letters*, 111:106617, 2021.

[13] Russell T W Prem K, Liu Y et al. The effect of control strategies to reduce social mixing on outcomes of the COVID-19 epidemic in Wuhan, China: a modelling study. *The Lancet Public Health*, 5(5):e261–e270, 2020.

[14] Li Q Hou X, Gao S et al. Intracounty modeling of COVID-19 infection with human mobility: Assessing spatial heterogeneity with business traffic, age, and race. *Proceedings of the National Academy of Sciences*, 118(24), 2021.

[15] Zhou L Lai S, Ruktanonchai N W et al. Effect of non-pharmaceutical interventions to contain COVID-19 in China. *Nature*, 585(7825):410–413, 2020.

[16] Eggo R M Davies N G, Kucharski A J et al. Effects of non-pharmaceutical interventions on COVID-19 cases, deaths, and demand for hospital services in the UK: a modelling study. *The Lancet Public Health*, 5(7):e375–e385, 2020.

[17] Cuevas E. An agent-based model to evaluate the COVID-19 transmission risks in facilities. *Computers in Biology and Medicine*, 121:103827, 2020.

[18] Xia S Liu Y, Gu Z et al. What are the underlying transmission patterns of COVID-19 outbreak? An age-specific social contact characterization. *EClinicalMedicine*, 22:100354, 2020.

[19] Costabal F S Linka K, Peirlinck M et al. Outbreak dynamics of COVID-19 in Europe and the effect of travel restrictions. *Computer Methods in Biomechanics and Biomedical Engineering*, 23(11):710–717, 2020.

[20] Watmough J Dreessche P. Reproduction numbers and sub-threshold endemic equilibria for compartmental models of disease transmission. *Mathematical Biosciences*, 180(1-2):29–48, 2002.

[21] Pauline Shuai Z S, Van D D. Global stability of infectious disease models using Lyapunov functions. *SIAM Journal on Applied Mathematics*, 73(4):1513–1532, 2013.

[22] Rebaza J Bessey K, Mavis M et al. Global stability analysis of a general model of Zika Virus. *Nonautonomous Dynamical Systems*, 6(1):18–34, 2019.

[23] Rdvg E Rntab C, Jes D et al. Improved inference of time-varying reproduction numbers during infectious disease outbreaks-sciencedirect. *Epidemics*, 29:100356, 2019.

[24] Wu P Li Q, Guan X et al. Early transmission dynamics in Wuhan, China, of novel coronavirus–infected pneumonia. *New England Journal of Medicine*, 382(13), 2020.

[25] Kim J H Kang D, Choi H et al. Spatial epidemic dynamics of the COVID-19 outbreak in China. *International Journal of Infectious Diseases*, 94:96–102, 2020.

[26] Annan-Phan S Hsiang S, Allen D et al. The effect of large-scale anti-contagion policies on the COVID-19 pandemic. *Nature*, 584(7820):262–267, 2020.

[27] Zhang B, Liang S, Wang G et al. Synchronized nonpharmaceutical interventions for the control of COVID-19. *Nonlinear Dynamics*, 2021.

Supplementary Files

This is a list of supplementary files associated with this preprint. Click to download.

- SupplementaryMaterial20210722.docx